

## Cryo-Electron Microscopy Structures of Yeast Alcohol Dehydrogenase

Sai Rohit Guntupalli,<sup>#</sup> Zhuang Li,<sup>#</sup> Leifu Chang, Bryce V. Plapp, and Ramaswamy Subramanian\*



Cite This: *Biochemistry* 2021, 60, 663–677



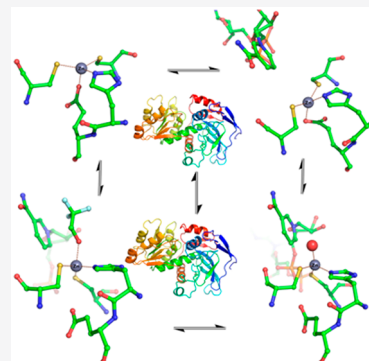
Read Online

ACCESS |

Metrics & More

Article Recommendations

**ABSTRACT:** Structures of yeast alcohol dehydrogenase determined by X-ray crystallography show that the subunits have two different conformational states in each of the two dimers that form the tetramer. Apoenzyme and holoenzyme complexes relevant to the catalytic mechanism were described, but the asymmetry led to questions about the cooperativity of the subunits in catalysis. This study used cryo-electron microscopy (cryo-EM) to provide structures for the apoenzyme, two different binary complexes with NADH, and a ternary complex with NAD<sup>+</sup> and 2,2,2-trifluoroethanol. All four subunits in each of these complexes are identical, as the tetramers have D2 symmetry, suggesting that there is no preexisting asymmetry and that the subunits can be independently active. The apoenzyme and one enzyme–NADH complex have “open” conformations and the inverted coordination of the catalytic zinc with Cys-43, His-66, Glu-67, and Cys-153, whereas another enzyme–NADH complex and the ternary complex have closed conformations with the classical coordination of the zinc with Cys-43, His-66, Cys-153, and a water or the oxygen of trifluoroethanol. The conformational change involves interactions of Arg-340 with the pyrophosphate group of the coenzyme and Glu-67. The cryo-EM and X-ray crystallography studies provide structures relevant for the catalytic mechanism.



X-ray crystallography of yeast (*Saccharomyces cerevisiae*) fermentative alcohol dehydrogenase (ADH1) crystallized with NAD<sup>+</sup> and trifluoroethanol shows that the subunits of the tetramer exist in two conformations. The tetramer has “back-to-back” dimers in which each dimer has one subunit in the open conformation, and the other subunit is in the closed conformation where the catalytic domain rotates ~12° toward the coenzyme binding domain and closes up the active site cleft.<sup>1,2</sup> Such a conformational change was observed first in horse liver alcohol dehydrogenase.<sup>3–5</sup> The active sites are on the “front” sides of the tetramer. The closed subunit of the asymmetric dimer binds NAD<sup>+</sup> and trifluoroethanol, and the alcohol is bound to the catalytic zinc with a geometry that resembles a Michaelis complex.<sup>1</sup> The open subunit has a conformation to which NAD<sup>+</sup> can bind and readily dissociate, but instead of water or alcohol bound to the zinc, the Glu-67 carboxylate binds to give an inverted coordination. This may represent an intermediate structure in the exchange of ligands bound to the zinc.<sup>2</sup> The glutamic acid residue is highly conserved in ADHs.<sup>6</sup> The inverted coordination was first observed in the dimeric human ADH3 and apoenzyme forms of the tetrameric, inducible *Escherichia coli* ADH.<sup>7–9</sup>

The asymmetry in the yeast ADH1 tetramer could be preexisting, or interactions of subunits in the crystal lattice could affect the conformations. Biochemical studies suggest that all four subunits can bind the coenzyme, but there are conflicting results and suggestions for negative cooperativity of subunits in catalysis, such as half-of-the-sites reactivity.<sup>1,10</sup>

Preexisting asymmetry has been suggested for the yeast cinnamyl alcohol dehydrogenase.<sup>11</sup> Now, cryo-electron microscopy (cryo-EM) can be used to determine the structures without crystallization, provide information about additional enzyme species in the catalytic mechanism, and test the origins of the crystallographic asymmetry. Cryo-EM structures for horse liver alcohol dehydrogenase complexed with NADH have been determined at ~2.7 Å resolution.<sup>12</sup>

In this study, structures were determined for commercial yeast alcohol dehydrogenase (ScbADH, from *Saccharomyces carlsbergensis*), which has substitutions of four amino acid residues but essentially the same enzyme kinetics compared to that of the laboratory strain.<sup>13</sup> Structures of the apoenzyme (protein with bound zincs but no coenzyme) and holoenzyme complexes with NADH or with NAD<sup>+</sup> and trifluoroethanol were found to have symmetric tetramers with either the open or the closed conformations observed by X-ray crystallography.

Received: November 24, 2020

Revised: January 7, 2021

Published: February 23, 2021



## MATERIALS AND METHODS

**Sample Preparation.** Commercial yeast ADH (EC 1.1.1.1, twice crystallized, lyophilized) was obtained from Worthington Biochemicals. This enzyme is prepared from the brewers yeast *S. carlsbergensis* and has an amino acid sequence that differs from that of the laboratory strain, *S. cerevisiae*, in the V58T, Q127E, Q147E, and I151V substitutions (GenBank entry FJ195977, UniProt entry B6UQED0). The apoenzyme sample was dissolved in 50 mM potassium phosphate buffer (pH 7.4), with 200 mM KCl, at a concentration of 5 mg/mL, clarified by centrifugation, and applied to a 24 mL column of Superdex S200 equilibrated with the same buffer at 5 °C. The protein in the major peak, at 13.3 mL, was collected and concentrated in an Amicon Ultra-0.5 centrifugal filter unit, and the concentration of protein was determined by using a calculated extinction coefficient of 1.33  $A_{280}$ /cm per milligram per milliliter. One major band was observed on 4–20% gradient sodium dodecyl sulfate gel electrophoresis.<sup>14</sup> Similarly, the enzyme–NADH complexes were prepared with 50 mM sodium phosphate buffer (pH 8.3) and brought to 2 mM disodium NADH without or with 200 mM 2,2,2-trifluoroethanol or 50 mM pyrazole. Trifluoroethanol and pyrazole are potent inhibitors, binding to the enzyme–NAD<sup>+</sup> complex, but dissociation constants for binding to the enzyme–NADH complex are not known. The cryo-EM maps of all of the samples prepared with NADH showed bound NAD(H), but none showed the presence of the inhibitors. The holoenzyme complex was prepared in 50 mM Tris-HCl buffer (pH 8.2), with 200 mM KCl, at 10 mg/mL protein with 4 mM free acid NAD<sup>+</sup> and 200 mM trifluoroethanol added in that order, and ~60 min elapsed before the samples were applied to the grids. The cryo-EM maps of this ternary complex showed both NAD and trifluoroethanol. The concentrations of ligands exceed the dissociation constants ( $K_i$  values) determined by enzyme kinetics (NAD<sup>+</sup>, 1.3 mM; NADH, 0.05 mM) and for binding to the enzyme–NAD<sup>+</sup> complex (2,2,2-trifluoroethanol, 2.8 mM; pyrazole, 0.011 mM).<sup>13,15,16</sup> The previous X-ray crystallography experiments used 1.7 mM 8-iodo-NAD<sup>+</sup> and 100 mM trifluoroethanol or 2 mM LiNAD<sup>+</sup> and 200 mM trifluoroethanol in 100 mM sodium *N*-tris(hydroxymethyl)-methyl-3-aminopropanesulfonate buffer (pH 8.4).<sup>1,2</sup> The free acid of NAD<sup>+</sup>, disodium NADH, 2,2,2-trifluoroethanol, and pyrazole were obtained from Sigma.

**Electron Microscopy.** Samples of the ScbADH apoenzyme (4  $\mu$ L, 5 mg/mL) were applied to glow-discharged Quantifoil holey carbon grids (Au, R1.2/1.3, 300 mesh). The ScbADH–NADH (trifluoroethanol) complex (4  $\mu$ L, 5 mg/mL) was applied to glow-discharged UltrAuFoil holey gold grids (R1.2/1.3, 300 mesh). The ScbADH–NADH (pyrazole) complex (4  $\mu$ L, 10 mg/mL) was applied to glow-discharged Quantifoil holey carbon (Au, R1.2/1.3, 300 mesh). The ternary complex of ScbADH with NAD<sup>+</sup> and trifluoroethanol (4  $\mu$ L, 10 mg/mL) was applied to glow-discharged Quantifoil holey carbon grids (Au, R1.2/1.3, 300 mesh). The grids were blotted for 2 s and plunged into liquid ethane using a Vitrobot. Cryo-EM data were collected with a Titan Krios microscope (FEI) operated at 300 kV, and images were collected using Leginon<sup>17</sup> at a nominal magnification of 81000 $\times$  (resulting in a calibrated physical pixel size of 1.05 Å/pixel) with a defocus range of −0.8 to −2.0  $\mu$ m. The images were recorded on a K3 electron direct detector in super-resolution mode at the end of a GIF-Quantum energy filter operated with a slit width of 20

eV. A dose rate of 20 electrons per pixel per second and an exposure time of 3.12 s were used, generating 40 movie frames with a total dose of ~54 electrons per angstrom.<sup>2</sup> Statistics for cryo-EM data are listed in Table 1.

**Table 1. Cryo-EM Data Collection, Refinement, and Validation Statistics**

	apoenzyme	NADH-O	NADH-C	NAD <sup>+</sup> -TFE
Data Collection and Processing				
no. of initial particle images	2323647	1746071	2675250	4630749
no. of final particle images	476561	429503	412250	1284904
map resolution (Å)	3.20	3.30	3.31	2.77
FSC threshold	0.143	0.143	0.143	0.143
map resolution range (Å)	3–3.8	3–3.8	3–3.8	2.4–2.8
Refinement				
initial model used	4W6Z	4W6Z	4W6Z	SENV
model resolution (Å)	3.2	3.2	3.3	2.8
model resolution range (Å)	3–3.8	3–3.8	3–3.8	2.4–2.8
map sharpening B factor (Å <sup>2</sup> )	−176	−80	−176	−170
model composition				
no. of non-hydrogen atoms	10332	10508	10196	10536
no. of protein residues	1388	1388	1388	1388
ligands	8 Zn	4 NADH, 8 Zn	4 NADH, 8 Zn	4 TFE, 4 NAD, 8 Zn
root-mean-square deviation				
bond lengths (Å)	0.010	0.006	0.008	0.011
bond angles (deg)	0.735	0.653	0.945	0.871
Validation				
MolProbity score	2.45	2.7	2.33	2.10
Clash score	7.0	14	4.97	7.17
poor rotamers (%)	4.0	4.0	8.2	2.99
Ramachandran plot (%)				
favored	94.0	93.0	94.64	95.07
allowed	6.0	7.0	5.07	4.93
disallowed	0.0	0.0	0.29	0.0
PDB entry	7KCQ	7KJY	7KC2	7KCB

**Image Processing.** The movie frames were imported into RELION-3<sup>18</sup> and aligned using MotionCor2 with a binning factor of 2.<sup>19</sup> Contrast transfer function (CTF) parameters were estimated using Gctf.<sup>20</sup> A few thousand particles were autopicked without a template to generate two-dimensional (2D) averages for subsequent template-based autopicking. The autopicked and extracted particle data sets were split into batches for 2D classifications, which were used to exclude false and bad particles that fall into 2D classes. Particles damaged on the air–water interface that are unavoidably picked by the autopick program needed to be excluded to obtain the best resolution maps. Particles from different views were used to generate an initial model in cryoSPARC.<sup>21</sup> Three-dimensional (3D) classification was further used to distinguish different compositional and conformational heterogeneity. A homogeneous data set was used for 3D refinement with no symmetry

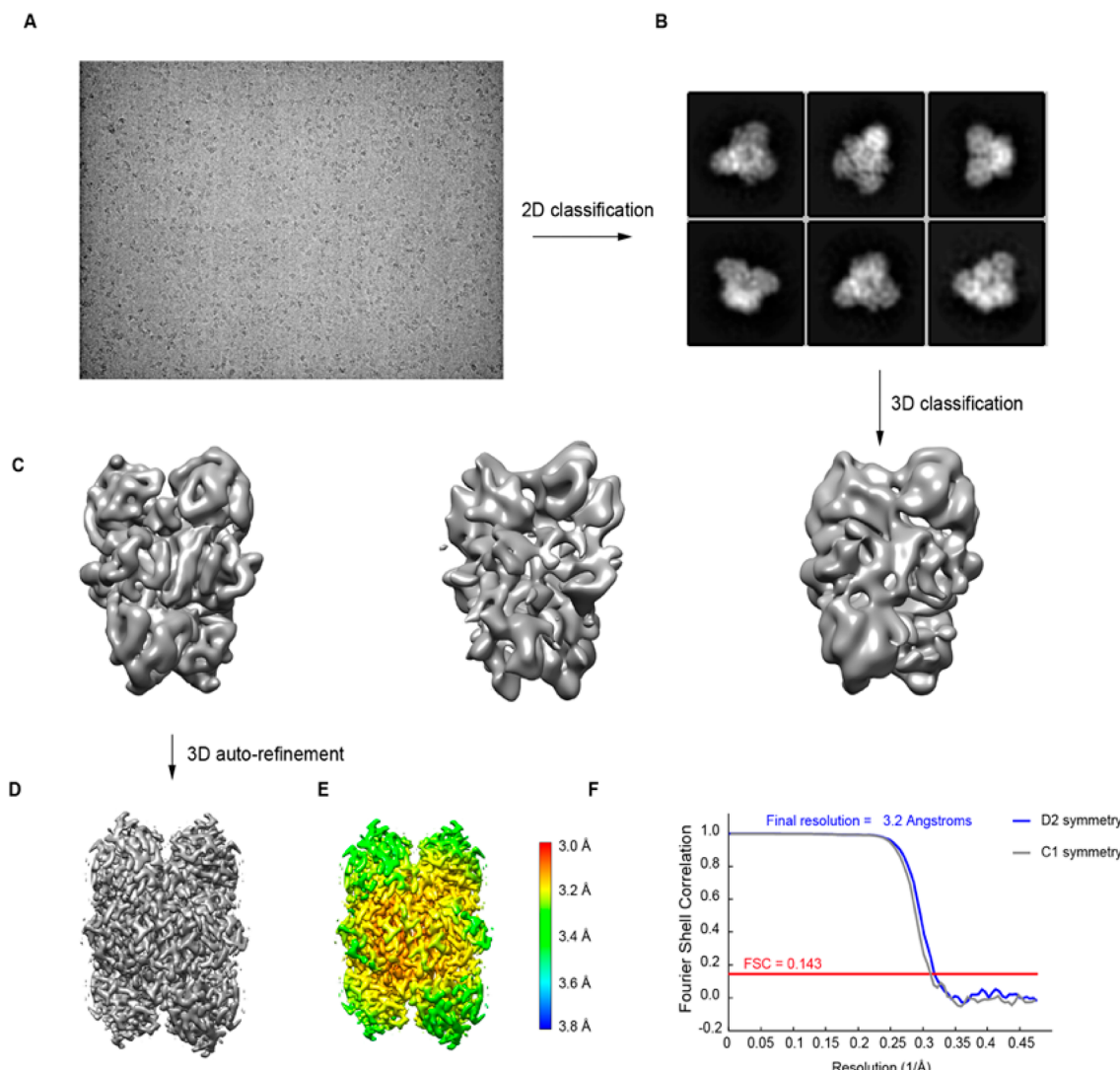


**Figure 1.** Cryo-EM of the apoenzyme ScbADH. (A) Representative raw cryo-EM micrograph. (B) Representative 2D class averages. (C) Major classes from 3D classification. (D) 3D refinement for particles from 3D classification as indicated. (E) Local resolution map for the reconstruction in panel D. (F) FSC plot of reconstructions with C1 and D2 symmetry.

imposed. Because the resulting maps did not show any signs of asymmetry among the subunits, 3D refinement was performed with D2 symmetry. Bayesian polishing and CTF refinement were performed to further improve the resolution.

For the apoenzyme ScbADH data set, 2323647 particles were autopicked and extracted from 2153 dose-weighted micrographs; 1094904 particles were selected from 2D classification and used for 3D classification, from which 476561 particles were selected and used for the final 3D refinement.

For the ScbADH–NADH (open, trifluoroethanol) data set, 1746071 particles were autopicked and extracted from 2161 dose-weighted micrographs; 771475 particles were selected from 2D classification and used for 3D classification, from which 429503 particles were selected and used for the final 3D refinement.

For the ScbADH–NADH (closed, pyrazole) data set, 2675250 particles were autopicked and extracted from 1541 dose-weighted micrographs; 796674 particles were selected from 2D classification and used for 3D classification, from

which 412250 particles were selected and used for the final 3D refinement.

For the ScbADH–NAD<sup>+</sup>–TFE data set, 4630749 particles were autopicked and extracted from 2260 dose-weighted micrographs; 2410860 particles were selected from 2D classification and used for 3D classification, from which 1284904 particles were selected and used for 3D refinement in cryoSPARC with D2 symmetry. Bayesian polishing used Relion, and the final 3D refinement used cryoSPARC with D2 symmetry and with C1 symmetry in parallel for comparison.

Cryo-EM image processing is summarized in Table 1. For all data sets, the magnification was set to 81000, the voltage to 300 kV, and the electron exposure to 54 e<sup>-</sup>/Å<sup>2</sup>. The defocus range was 0.8–2.0 μm; the pixel size was 1.05 Å, and the final symmetry imposed was D2.

**Model Building and Refinement.** The initial models for docking were from the structures determined and reported by X-ray crystallography. For the initial model of the ScbADH apoenzyme and the open NADH complex, subunit B of Protein Data Bank (PDB) entry 4W6Z<sup>1</sup> was split into two domains. Catalytic domain 1 consists of residues 1–156 and

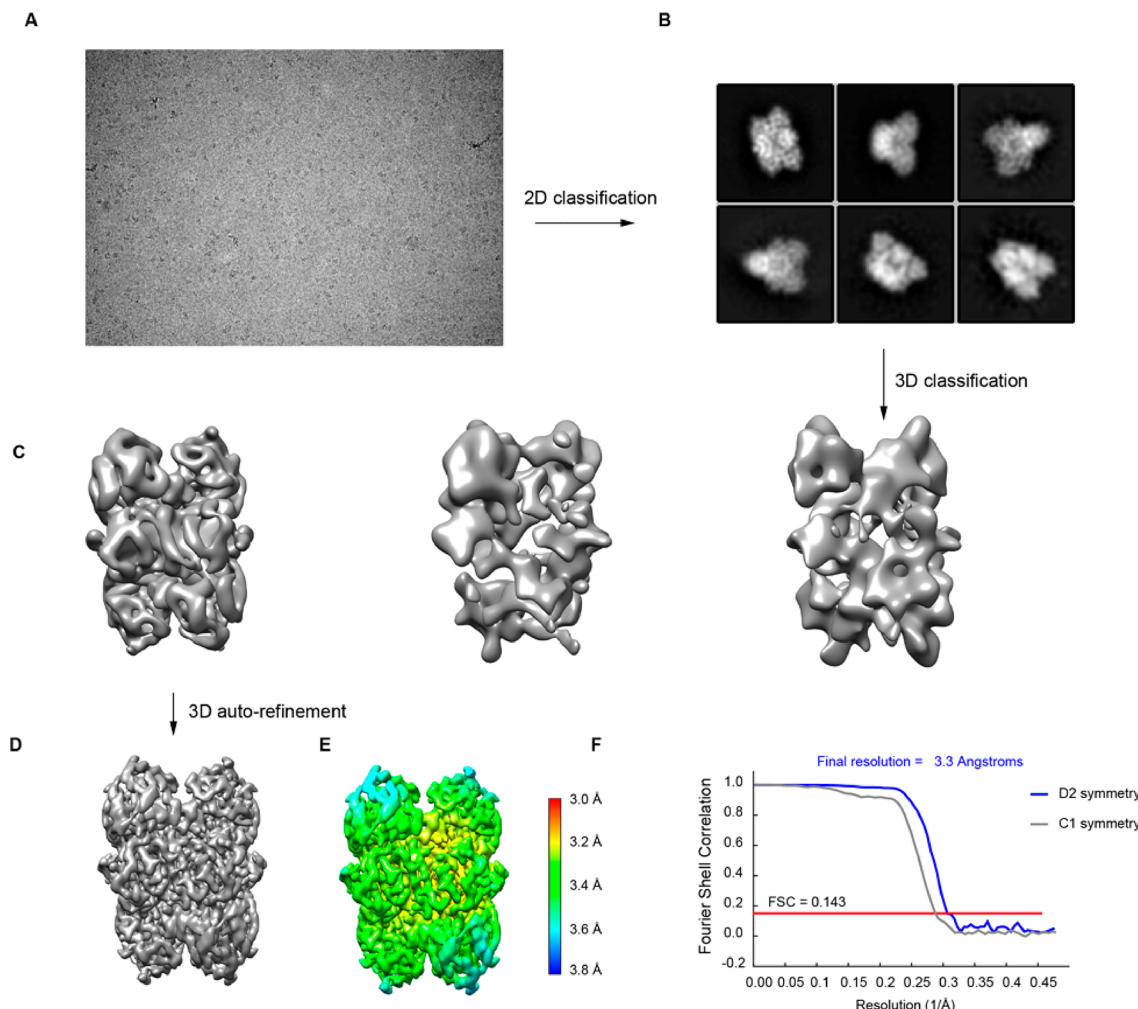


**Figure 2.** Cryo-EM of the ScbADH–NADH (open) complex. (A) Representative raw cryo-EM micrograph. (B) Representative 2D class averages. (C) Major classes from 3D classification. (D) 3D refinement for particles from 3D classification as indicated. (E) Local resolution map for the reconstruction in panel D. (F) FSC plot of reconstructions with C1 and D2 symmetry.

295–347 and the two  $Zn^{2+}$  atoms, and coenzyme binding domain 2 consists of residues 157–294. The maps were calculated with D2 symmetry with Relion,<sup>18</sup> and four copies of domain 1 were initially positioned. The fit to the map was visually inspected to confirm that the domains fit well into the maps. These coordinates were fixed, and four positions of domain 2 were docked using Phenix.<sup>22</sup> For the closed NADH and ScbADH–NAD<sup>+</sup>–TFE complexes, the coordinate sets for the two domains were created from subunit A of the reported enzyme–NAD<sup>+</sup>–TFE complex (PDB entry 5ENV).<sup>2</sup> The two domains for the tetramer were docked as described above.

For all of these structures, the two domains were also docked into the maps calculated in C1, followed by a round of real space rigid body refinement with each domain of each subunit as an independent unit. These monomer models were then used for real space refinement in the maps calculated with D2 symmetry. Structures were further refined using the real space refine mode in Phenix, and models were built using Coot.<sup>23</sup> The final details of the structures are listed in Table 1. The coordinates and maps of the four structures have been deposited in the PDB.

## RESULTS

**Structure Determination.** Particle picking was followed by 2D and 3D classifications as described above, 3D autorefinement, and map calculation within a mask in C1 symmetry and in D2 symmetry. For the apoenzyme, the particles were well dispersed and autopicking and processing allowed for map calculations (Figure 1). The final resolution of the map improved a little from C1 to D2, and the final map had a resolution of 3.2 Å as calculated from the FSC curve (Figure 1F). The resolution across the map varies from 3.8 to 3.0 Å. The initial model in the C1 map, after rigid body refinement (with four monomers), was then used to calculate the relationship between the monomers using the draw-rotation\_axis script in Pymol. The three 2-fold axes of rotation intersect at a common point perpendicular to each other. This confirmed the observation that averaging the map in D2 did not change the overall resolution, and the maps visually improved for the apoenzyme.

Similarly, the structure of the enzyme bound to NADH (open form) was determined, and the results are shown in Figure 2. The overall resolution improved as seen in the FSC curve (Figure 2F) with D2 symmetry. The overall resolution of the structure extended from 3.0 to 3.8 Å resolution as seen in the surface plot (Figure 2E) with a mean resolution of 3.2 Å.

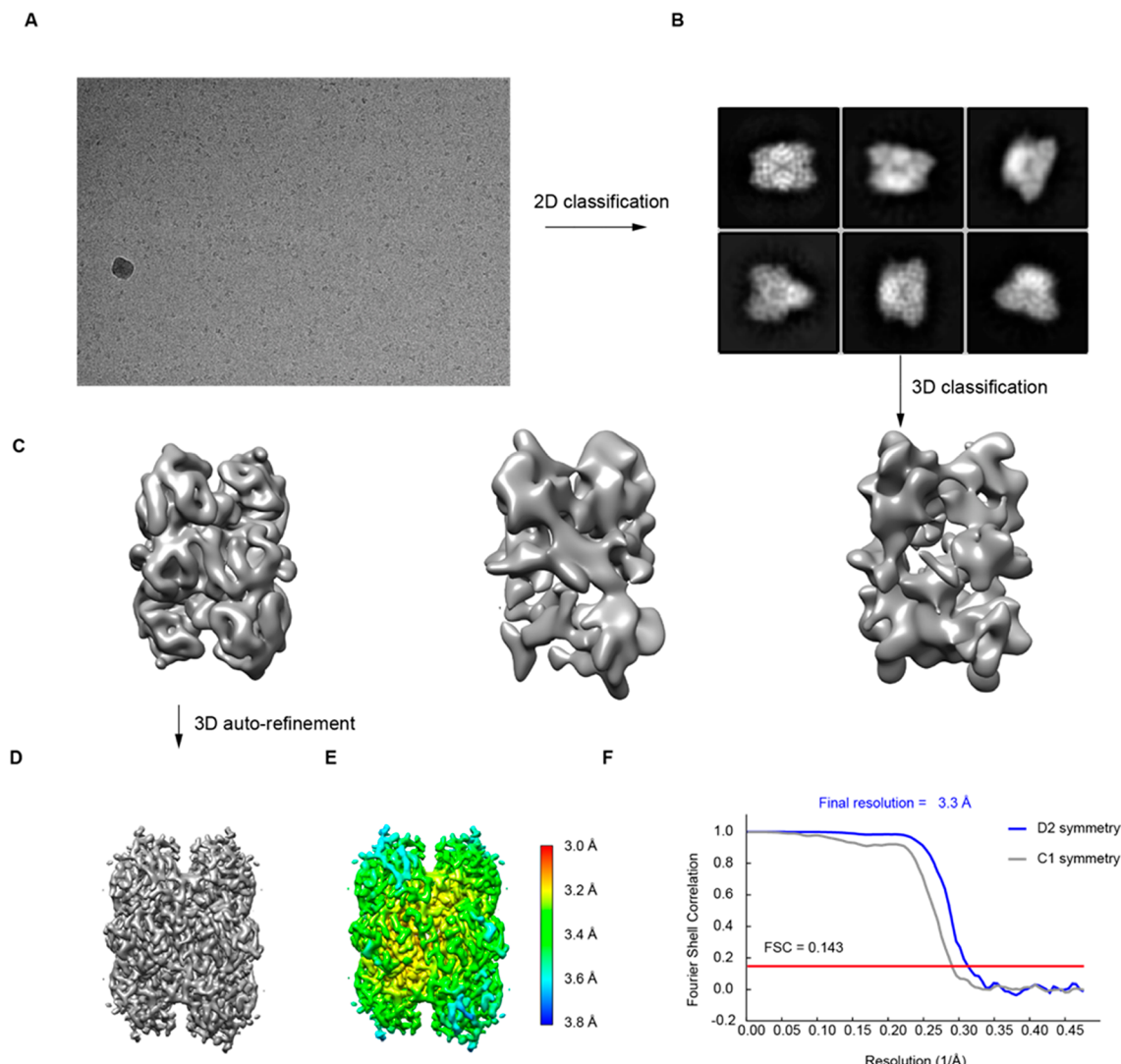


**Figure 3.** Cryo-EM of the ScbADH–NADH (closed) complex. (A) Representative raw cryo-EM micrograph. (B) Representative 2D class averages. (C) Major classes from 3D classification. (D) 3D refinement for particles from 3D classification as indicated. (E) Local resolution map for the reconstruction in panel D. (F) FSC plot of reconstructions with C1 and D2 symmetry.

The NADH was fit into the density after one round of real space refinement, before further rounds of model building and refinement.

The structure of the enzyme with NADH (closed form) had bound coenzyme, but the data did not show evidence for pyrazole in the binding pocket and instead showed a water molecule bound to the Zn. The overall resolution in this case improved to 3.3 Å when maps were calculated in D2 symmetry. The maps calculated in C1 and D2 did not show any differences in the active site or in the well-ordered regions, suggesting that there was no asymmetry in the particles used for the reconstruction (Figure 3).

For the ternary complex with NAD<sup>+</sup> and trifluoroethanol, the overall resolution was much better, at 2.77 Å. Again, the FSC plot clearly indicated improved resolution on averaging with D2 symmetry (Figure 4). The overall resolution might be better, and local changes could be made. To demonstrate that the binding of TFE was the same in all of the subunits, we confirmed the density for TFE in all four subunits in the map calculated in C1. The final results of the refinement and quality of the model are presented in Table 1 for all four structures.

**Quaternary Structures.** Each of the four new structures showed D2 symmetry, indicating that the subunits are experimentally identical. The tetrameric molecule is formed from two homodimers arranged “back to back” so that the active sites are exposed to solvent (Figure 5). The coenzyme binding domains (Rossmann fold, residues 157–294) in each subunit of a dimeric unit have extensive noncovalent interactions similar to those found in dimeric and other ADHs, as described previously.<sup>1,24</sup> The catalytic domains (residues 1–156 and 295–347) are connected to the coenzyme binding domains by two peptide bonds and by noncovalent interactions in the “hinge” around which the domains rotate to open or close the active site cleft between the domains.<sup>2</sup> The coenzyme binding domains of the two dimeric units form a core in the quaternary structures so that the catalytic domains in the open and closed forms are relatively free to move independently. The quaternary structures of the open and closed forms described here are similar.

**Zinc Coordination and Subunit Conformations.** The apoenzyme has an open conformation where the cleft between

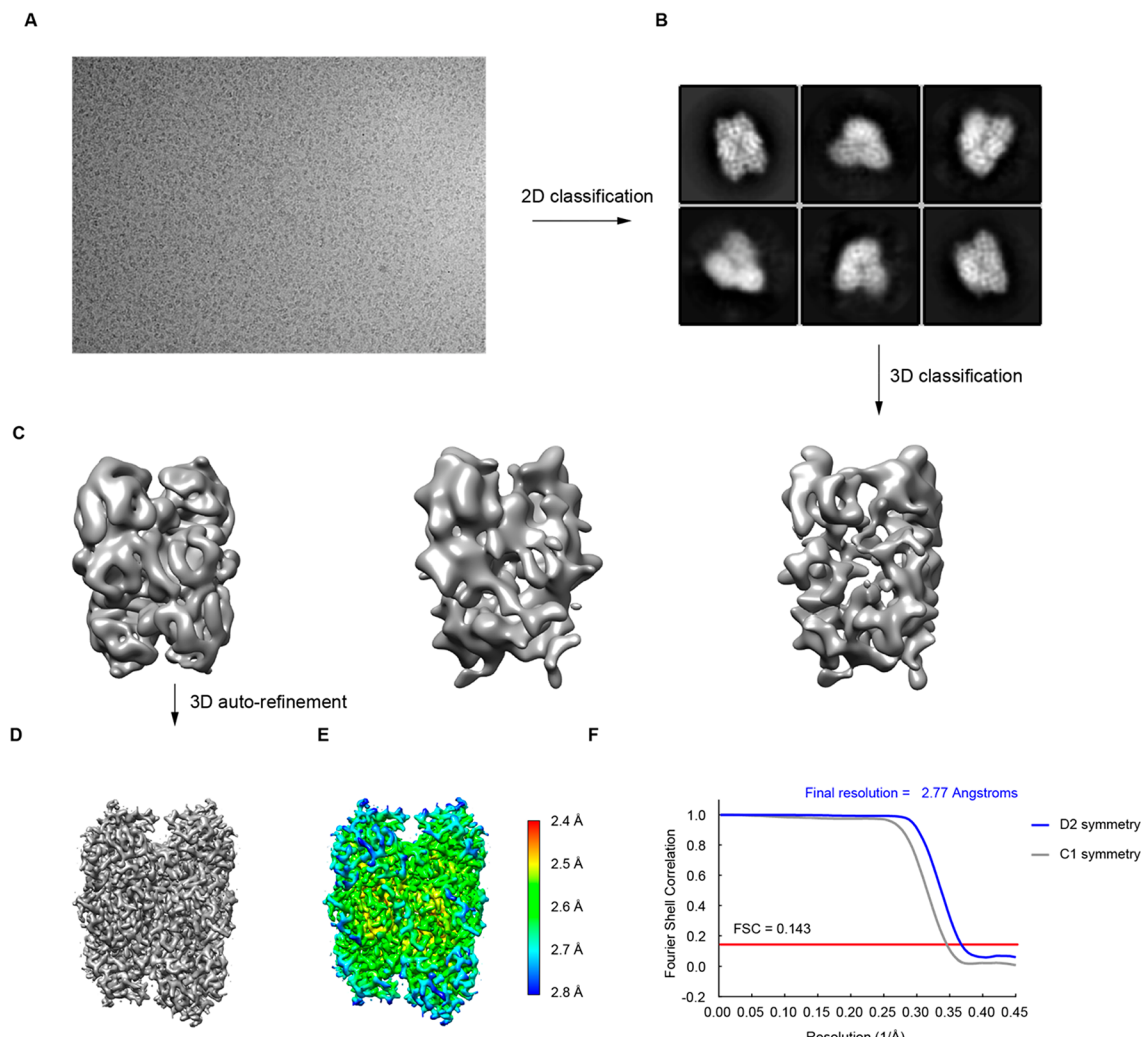


**Figure 4.** Cryo-EM of the ScbADH–NAD<sup>+</sup>–TFE ternary complex. (A) Representative raw cryo-EM micrograph. (B) Representative 2D class averages. (C) Major classes from 3D classification. (D) 3D refinement for particles from 3D classification as indicated. (E) Local resolution map for the reconstruction in panel D. (F) FSC plot of reconstructions with C1 and D2 symmetry.

the coenzyme and catalytic domains would allow coenzyme to bind, and the catalytic zinc has an “inverted” coordination with Cys-43, His-66, Cys-153, and Glu-67. This structure is similar to those of the apoenzyme forms determined by X-ray crystallography (PDB entry 4W6Z, subunits B and D, not shown; see Figure 2B of ref 1). One complex made with NADH also has an open conformation and the inverted zinc coordination (Figure 6A), and NADH is bound to the coenzyme binding domain in a position similar to that found for NAD<sup>+</sup> in the B chain subunit in the X-ray structure (PDB entry SENV<sup>2</sup>). The enzyme sample was prepared with NADH and trifluoroethanol, which could form an abortive complex, but there was no evidence of trifluoroethanol in the active site, apparently because the affinity is low.<sup>25</sup> Horse and human ADHs form abortive complexes with NADH and various alcohols, and the tetrameric ADH from *Pseudomonas aeruginosa* forms an abortive complex with NADH and ethylene glycol.<sup>26–28</sup> Another complex made with NADH alone had a lower resolution of 3.5 Å, but the same overall structure as the one prepared with NADH and trifluoroethanol (results not shown). Both of these structures represent the open form of the enzyme bound to the coenzyme with the inverted active site Zn coordination.

In contrast, the structure for the sample of the enzyme made with NADH and pyrazole has the closed conformation with NADH bound in the active site and the classical coordination of the zinc with a water (Figure 6B). There is no good evidence that pyrazole is bound to the zinc or to the nicotinamide ring. An adduct with NAD<sup>+</sup> and pyrazole forms with the yeast and liver enzymes (PDB entry 1N8K<sup>29</sup>), but the adduct does not form with NADH. The X-ray structure of the complex of the horse liver enzyme with NADH also has the closed conformation in the crystalline state and predominantly the classical zinc coordination with a water bound to the zinc (PDB entry 4XD2).<sup>30</sup> The ScbADH–NAD<sup>+</sup>–trifluoroethanol complex also has the closed conformation with the catalytic domain rotated toward the coenzyme binding domain and the classical coordination of the catalytic zinc with Cys-43, His-66, Cys-153, and the oxygen of the alcohol (Figure 6C). The structure of this complex is very similar to those determined by X-ray crystallography (PDB entry 4W6Z, subunits A and C; PDB entry SENV, subunit A).

The overall conformations of the open and closed forms of one subunit of ScbADH are illustrated in Figure 7. The coenzyme binding domains are very similar except that when coenzyme is bound, the ends of a few loops of the Rossmann

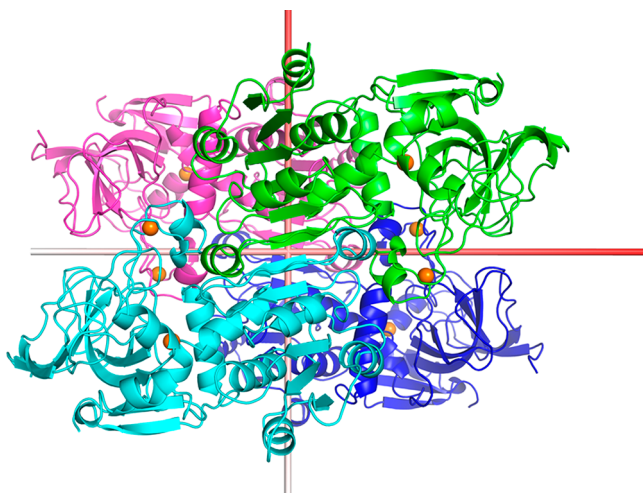


**Figure 5.** Quaternary structure of the apoenzyme. Each of the monomers is colored differently. The axes relating the different subunits are also shown. The view is down the 2-fold axis through the coenzyme binding domains of the dimeric unit. The three axes are perpendicular to each other and meet in the center of the molecule. The orange spheres show the positions of the Zn atoms.

fold are altered. Likewise, the catalytic domains are similar, except that the coordination of the catalytic zinc is altered, and positions of residues interacting with the coenzyme have moved. The active site cleft is closed in the ternary complex.

**Comparison of Tertiary Structures Determined by Cryo-EM and X-ray Crystallography.** The structures that were determined by X-ray crystallography (PDB entries 4W6Z and SENV) showed asymmetry in the dimeric units where one subunit (B chain) has an open conformation and the catalytic zinc has the inverted, alternative coordination with Cys-43, His-66, Cys-153, and Glu-67, whereas the other subunit (A chain) contains NAD<sup>+</sup> and 2,2,2-trifluoroethanol in the closed conformation with the classical coordination of the catalytic zinc with Cys-43, His-66, Cys-153, and the oxygen of the alcohol. The X-ray and cryo-EM structures were compared by superpositioning the subunits, then the coenzyme binding domains, and then the catalytic domains to calculate the relative domain closure as given in Table 2. In the cryo-EM structures, the subunits in the apoenzyme (no coenzyme bound) and one complex with NADH have an open conformation where a small rotation ( $\sim 1^\circ$ ) superpositions the catalytic domains. The coenzyme binding domain of the complex with NAD<sup>+</sup> and TFE is very similar to that in the open complex with NADH, but the catalytic domain is rotated  $\sim 10^\circ$  closer to the coenzyme binding domain in the ternary complex, for a total of  $\sim 11^\circ$  as compared to the apoenzyme. The closed form of the complex with NADH is very similar to that of the complex with NAD<sup>+</sup> and trifluoroethanol, requiring only  $\sim 1^\circ$  rotation to superposition the catalytic domains. The subunits of the apoenzyme and the open complex with NADH have a somewhat more open conformation than the open conformations (B subunit) of the crystal structures (PDB entry 4W6Z or SENV). In contrast, the subunits of the complexes with NAD<sup>+</sup> and trifluoroethanol are very similar [root-mean-square deviation (RMSD) of 0.4 Å] to the structure of the closed conformation (A subunit) of the crystal structure.

The coenzyme binding domains of the open conformations are very similar, but the complexes with bound coenzyme differ in some loops as compared to those domains without bound

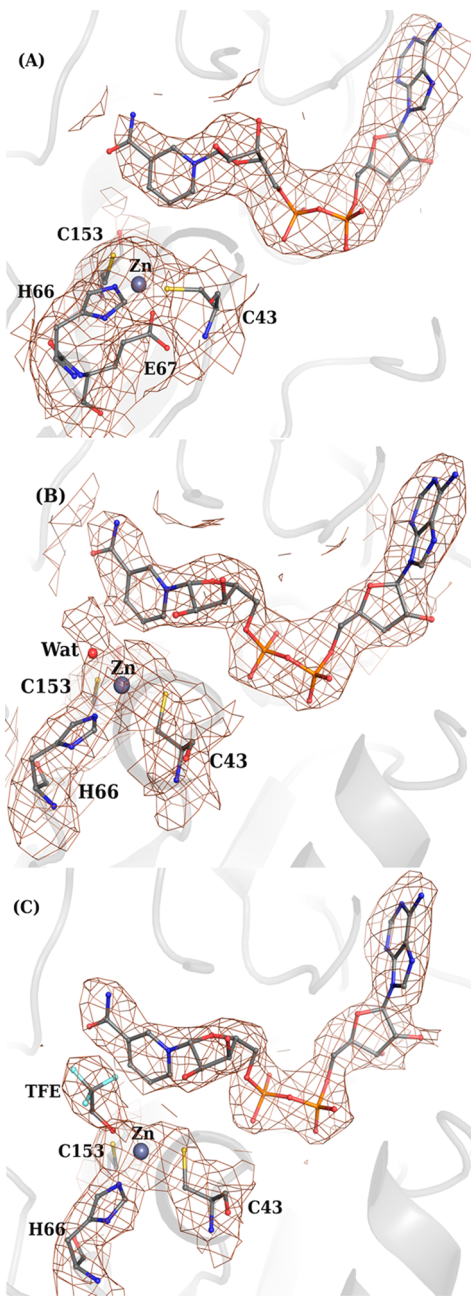


**Figure 6.** Coordination of the active site zinc and coenzyme binding. (A) Cryo-EM map for the open conformation of a complex with NADH showing that the catalytic zinc is coordinated to Glu-67 (PDB entry 7KJY). (B) Closed conformation of a complex with NADH that has the classical coordination of the catalytic zinc with water bound to the zinc (PDB entry 7KC2). (C) Enzyme–NAD<sup>+</sup>–trifluoroethanol (TFE) complex that has the classical coordination of the active site zinc with the oxygen of the alcohol (PDB entry 7KCB).

coenzyme. In particular, Gly-180 and Gly-181 are flipped so that Gly-181 N interacts with coenzyme pyrophosphate O1N, and the loops with Val-247, Ser-248, and Gly-269–Ala-272 have shifted to accommodate the nicotinamide ribose. Similar differences were observed in the open conformation of the B subunit (PDB entry 4W6Z) with no coenzyme bound and the B subunit (PDB entry SENV) that has bound coenzyme. These local conformational changes result from the interactions with coenzyme.

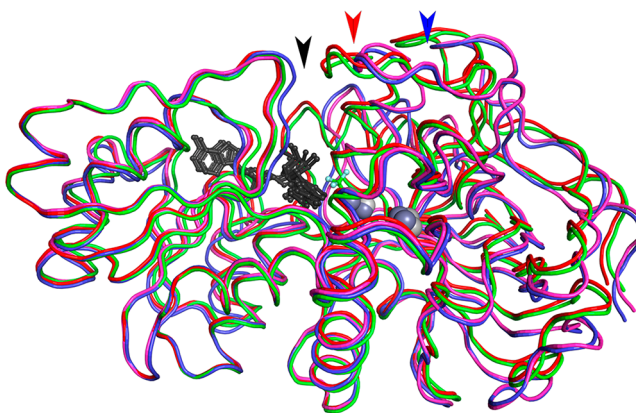


**Figure 7.**  $\alpha$ -Carbon backbone of one subunit with coenzyme binding domains superpositioned. Apoenzyme in the open conformation (blue), the complex with NADH in the open conformation (magenta) and closed conformation (red), and the closed conformation of the holoenzyme complex with NAD<sup>+</sup> and trifluoroethanol (green). The black arrow shows the cleft. The red arrow points to changes in the loop, including amino acid residue 55, and the blue arrow to the loop with residue 16.

**Table 2. Comparisons of Tertiary Structures<sup>a</sup>**

fixed unit, superpositioned unit, PDB entry, ligands and subunit	subunit RMSD (Å)	coenzyme RMSD (Å)	catalytic RMSD (Å) <sup>b</sup>	rotation <sup>b</sup> (deg)
7KCQ apo, 7KJY NADH-O	0.55	0.69	0.45	1.1
7KJY NADH-O, <sup>c</sup> 7KCB NAD <sup>+</sup> -TFE	1.48	0.35	0.77	10.2
7KCQ apo, 7KCB NAD <sup>+</sup> -TFE	1.6	0.76	0.70	11
7KC2 NADH-C, <sup>c</sup> 7KCB NAD <sup>+</sup> -TFE	0.38	0.34	0.33	1.3
4W6Z apo B, 7KCQ apo	0.70	0.51	0.55	2.8
4W6Z apo B, 7KJY NADH-O	0.86	0.87	0.58	3.2
SENV NAD <sup>+</sup> B, 7KJY NADH-O	0.76	0.46	0.69	2.4
4W6Z NAD <sup>+</sup> -TFE A, 7KCB NAD <sup>+</sup> -TFE	0.40	0.41	0.37	0.67
4W6Z apo B, 4W6Z NAD <sup>+</sup> -TFE A	1.9	0.94	0.86	12

<sup>a</sup>The  $\alpha$ -carbon atoms were superpositioned with the program O,<sup>31</sup> and the RMSD in angstroms is reported.<sup>31</sup> The coenzyme binding domain includes residues 157–294, and the catalytic domain includes residues 1–156 and 295–347. <sup>b</sup>After the coenzyme binding domains were superpositioned, the catalytic domains were superpositioned, and the rotation of the catalytic domain toward the coenzyme binding domain was calculated. <sup>c</sup>NADH-O has the open conformation, and NADH-C has the closed conformation.

The catalytic domains for the open conformations are very similar among the enzymes, with the inverted coordination of the catalytic zinc. The catalytic domains of the closed conformations of the ternary complexes are also similar, and the catalytic zinc has the classical coordination.

**Origins of Asymmetry.** All four structures determined by cryo-EM show that the four subunits in the tetramer are experimentally identical. All four subunits in the apoenzyme and in one complex with NADH have the open conformation, and the subunits in another complex with NADH and the NAD<sup>+</sup>-trifluoroethanol complex have the closed conformation. In contrast, the structures determined by X-ray crystallography (PDB entries 4W6Z and SENV) have

asymmetric dimeric units where one subunit, B chain, with or without coenzyme, is open and the other subunit, A chain, with NAD<sup>+</sup> and trifluoroethanol, is closed. The tetramer is formed with two back-to-back, symmetry-related AB dimers to form an AB:AB tetramer. The asymmetry in the dimer could be preexisting for the enzyme in solution or because of crystal lattice interactions. Crystallography of yeast cinnamyl dehydrogenase suggested that the asymmetry of dimers was preexisting and resulted in “half-of-the-sites” reactivity, but there is no good kinetic evidence for cooperativity in yeast alcohol dehydrogenase.<sup>11</sup>

The interactions in the tetramers in the structures previously determined by crystallography were examined for potential origins of asymmetry.<sup>2</sup> Modeling of a symmetric dimer by replacing the B subunit with an A subunit (superpositioning the coenzyme binding domains) did not generate any serious steric conflicts within the tetramer, and now the structure from cryo-EM for the NAD<sup>+</sup>-trifluoroethanol complex confirms that steric hindrance would not prevent formation of symmetric holoenzyme tetramers. The modeled AA dimer superpositions very closely on the cryo-EM dimer with an RMSD of 0.56 Å, but the cryo-EM structure is more compact by ~0.5 Å for the ~100 Å end-to-end distance between  $\beta$ C atoms of Glu-4. In the observed AB asymmetric dimer, the distance is ~101 Å. Nevertheless, the rotation of the catalytic domain moves the Glu-4  $\beta$ C ~7 Å and would alter the crystal lattice contacts observed for the open B subunit. Superpositioning of the cryo-EM structure of the ternary complex in the crystal lattice and generating symmetry-related molecules shows steric clashes in the loops with residues 84–87, 141, and 142, and favorable electrostatic interactions of residues 17, 330, and 331 in subunit B would be lost. It appears that the crystal lattice may stabilize the B subunit in the open conformation even when coenzyme and trifluoroethanol are bound (PDB entry SENV). The binding of NAD<sup>+</sup> and trifluoroethanol drives the conformational changes in all subunits in solution, but the interactions in the crystal lattice apparently can offset those energetics.

**Primary and Secondary Structures.** The *S. carlsbergensis* enzyme differs at four amino acid residues from the *S. cerevisiae* enzyme studied by crystallography, but the differences were not expected to affect the structures. The substitutions (*S. cerevisiae* to *S. carlsbergensis*) of V58T, Q127E, and Q147E are not readily distinguishable at the current resolutions, and the local structures are not significantly altered. The I151V substitution is confirmed in the maps, but the removal of the methyl group has only weak effects on the structure of the neighboring residues, as has been found for similar substitutions of aliphatic amino acids in horse liver alcohol dehydrogenase.<sup>32,33</sup>

The cryo-EM and crystallographic studies both show that a disulfide bond is formed between the two symmetry-related Cys-277 residues of the subunits in the dimeric unit. In living yeast, it is estimated that 17% of Cys-277 (or Cys-278) is oxidized, but under redox stress from added H<sub>2</sub>O<sub>2</sub>, 40% can be oxidized.<sup>34</sup> Apparently, the bond forms readily during the purification of the enzyme under aerobic conditions. The bond stabilizes the enzyme against heat denaturation, as shown by the 20 °C decrease in melting temperature (from  $t_{50}$  ~58 °C) after treatment with dithiothreitol, which increases the activity of the enzyme somewhat.<sup>1,35</sup>

**Coupling of Changes in Conformation and Zinc Coordination.** The apoenzyme has the open conformation

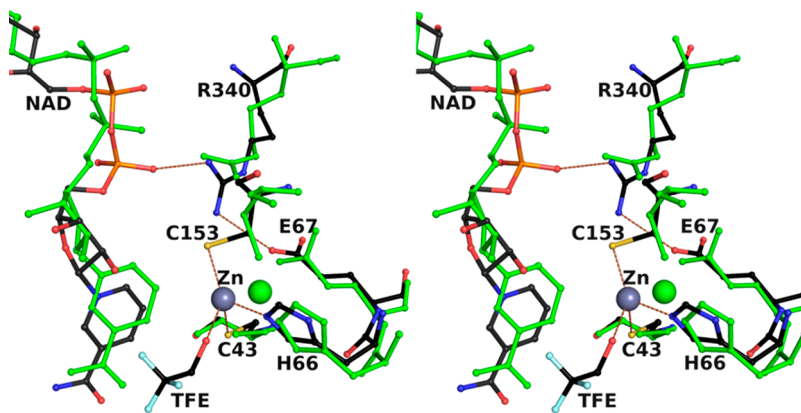


**Figure 8.** Stereoview of the active sites of the ternary complex superpositioned on the open complex with NADH. The structure (PDB entry 7KCB) of the closed ScbADH–NAD<sup>+</sup>–trifluoroethanol (TFE) complex is shown as balls and sticks with atom coloring and dashed lines to indicate interactions. The structure (PDB entry 7KJY) of the open complex with NADH is colored green and shown as sticks. The inverted coordination of the zinc is the same in the apoenzyme and the complex with NADH; however, the oxygen of the trifluoroethanol displaces Glu-67 in the holoenzyme complex, and Glu-67 interacts with Arg-340.

**Table 3. Interactions of Glu-67 and Arg-340 in the Enzyme Forms<sup>a</sup>**

	apoenzyme	NADH-O	NAD <sup>+</sup>	NAD <sup>+</sup> -TFE	NADH-C
PDB entry	7KCQ, 4W6Z	7KJY	SENV	7KCB, 4W6Z, SENV	7KC2
Zn–Glu-67 OE2	2.0, 2.2	2.3	2.6	3.8, 4.9, 5.0	4.0
Glu-67 OE2–Arg-340 NH2	3.6, <sup>b</sup> 4.8	4.1 <sup>b</sup>	4.5	2.9, 2.8, 2.6	3.0
Arg-340 NH1–NAD O2N	—	3.9	3.4	2.6, 2.7, 3.1	2.8

<sup>a</sup>Distances between atoms in angstroms. Averages of subunits B and D from PDB entry 4W6Z for the apoenzyme and subunits A and C for the holoenzyme. NADH-C is the closed conformation, and NADH-O is the open conformation. <sup>b</sup>Fitting to the map is not definitive.

with an inverted coordination of the catalytic zinc (PDB entries 7KCQ and 4W6Z, subunit B), and NAD<sup>+</sup> can bind with only small changes in structure (PDB entry SENV, subunit B) or NADH (PDB entry 7KJY). After NADH or NAD<sup>+</sup> binds, the conformation closes and the zinc binds water (PDB entry 7KC2) or an alcohol in the classical coordination (PDB entry 7KCB). It appears that the binding of coenzyme would facilitate the change in zinc coordination because the interaction of the catalytic zinc with Glu-67 is altered when its carboxyl group moves to interact with the guanidinium group of Arg-340, which interacts with the coenzyme pyrophosphate (Figure 8). The homologous arginine residue is highly conserved in ADHs.<sup>6</sup> In the structures of the yeast apoenzyme and the open complex with NADH (PDB entry 7KJY), Glu-67 interacts with the zinc, but not with Arg-340. In the holoenzyme structures with NAD<sup>+</sup> and trifluoroethanol, Glu-67 interacts with Arg-340 (PDB entries 4W6Z, SENV, and 7KCB) and is not ligated to the zinc. Nevertheless, there is space for Glu-67 to transiently coordinate to the zinc, displacing the zinc-bound water and facilitating the binding of the substrate (alcohol or aldehyde) to an enzyme–coenzyme complex when the oxygen of the substrate displaces the oxygen of Glu-67. The binding of the coenzyme and the movements of Glu-67 and Arg-340 appear to be coupled to the changes in protein conformation and zinc coordination. Table 3 summarizes the interaction distances in the various complexes.

## DISCUSSION

**Early History.** An electron microscopic study of yeast ADH in crystalline flakes isolated from anaerobically grown *S. carlsbergensis* cells, together with small-angle X-ray scattering of the isolated enzyme, proposed that the enzyme has four

subunits arranged tetrahedrally. The longest dimension was 9.1 nm, and the shortest was 7.9 nm.<sup>36</sup> The crystallographic space group was suggested to be *P*312, which is consistent with the *P*321 space group in the X-ray crystallography and cryo-EM studies, where a long dimension of ~10 nm was found.<sup>1,2,37</sup> The studies presented here provide atomic details about four different structures of the enzyme that are not in a crystalline state but can represent soluble forms that are active in the cytoplasm.

**Conformational Changes, Asymmetry, and Zinc Coordination.** Although the structures determined by X-ray crystallography and electron microscopy revealed differences in the symmetry of the tetramers, the significant result is that similar open and closed conformations of the subunits were observed with each type of experiment. The crystals for the first structure (PDB entry 4W6Z) were formed in hanging drops with 8-iodo-NAD<sup>+</sup> with trifluoroethanol and shipped to the synchrotron in stabilizing fluid that contained 30% MPEG-5000 and 0.5 M trifluoroethanol, but no added NAD<sup>+</sup>, and coenzyme remained bound in the closed conformation of one subunit of the dimeric unit; however, no coenzyme was bound to the open conformation of the other subunit. In contrast, for the second structure (PDB entry SENV), NAD<sup>+</sup> and 0.28 M trifluoroethanol were added for shipping, and NAD<sup>+</sup> was found in the the open and closed subunits. Apparently, the closed conformation binds coenzyme tightly, whereas the open conformation allows coenzyme to dissociate. The cryo-EM studies found open conformations for the apoenzyme and one complex with NADH, similar to those determined by X-ray crystallography, as shown in Table 2. Likewise, similar closed conformations for the complexes with NAD<sup>+</sup> and trifluoroethanol were found by cryo-EM and crystallography, and cryo-EM found another complex with NADH in the closed

form. The cryo-EM studies showed that all complexes had D2 symmetry, indicating that all four subunits in each complex are identical. Examination of the structures suggests that each subunit can be independently catalytically active, as the conformational change would not affect interactions of the catalytic domains among subunits.<sup>1</sup>

The asymmetry observed in the crystallography studies reflects different energetically accessible states, which may be related to crystal packing.<sup>1</sup> This implies that the energetics of the conformational change are modest. Calculations of the energetics of the conformational change of the apoenzyme of horse liver alcohol dehydrogenase from open to closed suggest the difference is approximately +10 kcal/mol, but the energetics of the holoenzyme complexes must favor the closed conformation.<sup>38</sup> The complexes of horse liver ADH with NADH, NADH and formamides, or NAD<sup>+</sup> and trifluoroethanol have the closed conformation in the crystals.<sup>30,39</sup> Given the dissociation constants for NAD<sup>+</sup> and trifluoroethanol (27 and 8.4 μM, respectively), the formation of the ternary complex with horse ADH1E has a free energy change of approximately −13 kcal/mol. For the yeast enzyme, with a lower affinity for the ligands, the free energy change is approximately −6 kcal/mol for binding NADH and approximately −7 kcal/mol for binding NAD<sup>+</sup> and trifluoroethanol. The energetics of the conformational change in solution might be similar to those arising from the contacts in the crystal lattice. The open and closed conformations of the yeast enzyme bound to NADH were observed with cryo-EM, suggesting that the energies of these forms are similar.

Structures of various ADHs determined by X-ray crystallography show symmetry or asymmetry in the relationship of subunits in the biological molecule and changes in zinc coordination in complexes. The apoenzyme of horse liver ADH1E has a crystallographic axis of symmetry relating the two subunits in the dimer, but holoenzyme complexes (~35 structures) typically have a dimer as the asymmetric unit, where a molecular 2-fold axis relates very similar subunit structures.<sup>3,4</sup> For instance, for the atomic resolution structure (1.14 Å) of the ternary complex of ADH1E with NAD<sup>+</sup> and pentafluorobenzyl alcohol, α-carbon atoms of one subunit of the dimer can be superpositioned on the other subunit with an RMSD of 0.17 Å with differences of ≤1 Å in distant residues of the catalytic domain.<sup>39</sup> The cryo-EM structure of the closed conformation of horse liver ADH1E complexed with NADH refined best with C2 symmetry; however, 10 structures were modeled, and refinement is not complete.<sup>12</sup> The X-ray structure (1.1 Å) of ADH1E complexed with NADH shows the closed conformation with a water bound to the zinc, which appears to have alternative positions.<sup>30</sup> The dimeric cod liver ADH1 complexed with NAD has one subunit in an open conformation and the other subunit in a closed conformation, with the classical zinc coordination in both subunits.<sup>40</sup> A holoenzyme complex of dimeric human ADH3 (glutathione-dependent formaldehyde dehydrogenase) has one subunit with NADH and the substrate in a closed conformation and the classical zinc coordination, whereas the other subunit has NADH bound in an open conformation and the inverted zinc coordination.<sup>41</sup> The apoenzyme form of the dimeric ADH from *Arabidopsis thaliana* has identical subunits with partially open conformations, but a holoenzyme complex has one subunit in a closed conformation with bound NAD and the other subunit with a more open conformation and no NAD bound.<sup>42</sup> It was argued that the asymmetry in the complex with

NAD was not caused by crystal lattice interactions. The dimeric *S. cerevisiae* cinnamyl ADH is asymmetric.<sup>11</sup> In these dimeric enzymes, the apoenzyme and ternary complexes have the classical coordination of the zinc, but various binary complexes show evidence of the inverted coordination.

In contrast, the apoenzyme forms of the tetrameric enzymes have the inverted coordination of the catalytic zinc whereas various complexes have the classical coordination. The tetrameric enzymes have ~27 fewer amino acid residues than the dimeric enzymes, mostly in one region, but the overall conformations of the subunits and zinc coordination are similar.<sup>1,5,6</sup> The tetrameric *E. coli* ADH (37% identical to yeast ADH1) has the inverted coordination of zinc with Glu-59 in three of the four subunits of the apoenzyme, but one subunit has the classical coordination with the zinc water; another structure with NAD bound to all four subunits has a tetramer with ~222 symmetry, and the zinc has the classical coordination with a water.<sup>8,43</sup> The open, apoenzyme form of the tetrameric ADH from *Bacillus stearothermophilus* crystallized from 12% trifluoroethanol has 222 noncrystallographic symmetry, and the catalytic zinc atoms in two subunits bind trifluoroethanol in the classical coordination; however, the other two subunits show evidence of the alternative coordination of the zinc with Glu-62.<sup>44</sup> The ADH from the hyperthermophile *Sulfolobus solfataricus* (31% identical to yeast ADH1) has crystallographic 222 symmetry in the apoenzyme, with the inverted coordination of the catalytic zinc with Glu-69.<sup>45</sup> The ternary complex crystallized with NAD<sup>+</sup>, 2,2,2-trifluoroethanol, and 2-ethoxyethanol shows a closed conformation (rotation of 11° relative to apoenzyme), with ~222 symmetry and a classical coordination with 2-ethoxyethanol bound to the zinc and NAD<sup>+</sup> (or NADH) in all four subunits.<sup>46</sup> The tetrameric *Aeropyrum pernix* ADH has 222 symmetry in the complex with NADH and octanoic acid, which is bound to the catalytic zinc in the classical coordination.<sup>47</sup> The complex of *P. aeruginosa* ADH with NADH and ethylene glycol has ~222 symmetry with the classical coordination of the zinc.<sup>28</sup> The *Cupriavidus necator* JMP134 ADH reduces furfural with NADH, and the apoenzyme has ~222 symmetry with the inverted zinc coordination in the open conformation but crystallizes with NADH bound to two subunits with a closed conformation and the classical coordination of the zinc with a bound water or substrate, which is similar to the asymmetric structure of yeast ADH determined by X-ray crystallography.<sup>48</sup>

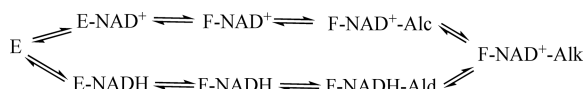
The origins of asymmetry and kinetic evidence for negative cooperativity in catalysis by alcohol dehydrogenases have not been established. The cryo-EM results for the yeast enzyme suggest that the various complexes can be symmetric and that the subunits can act independently.

There is no basis to suggest that the yeast enzyme has cooperativity among the subunits, or “half-of-the-sites” reactivity that was proposed on the basis of some studies that found fewer than four subunits per tetramer could bind NADH.<sup>10</sup> Loss of zinc atoms, oxidation of sulphhydryl groups, and dissociation into dimers can contribute to the diminished stoichiometry. Yeast ADH is a tetramer, but it loses activity when it dissociates into dimers or monomers, as determined by gel filtration (unpublished observations), indicating that subunit interactions are important. In multimeric enzymes, when one subunit binds substrates and changes conformation, the energetics of interacting subunits must change, even if the effects have not been determined by various techniques.

Structures of complexes with substoichiometric occupancies of ligands might show evidence of interactions and cooperativity.

**Catalytic Mechanism.** The X-ray and cryo-EM studies provide structures that are relevant for the predominantly ordered catalytic mechanism of yeast and horse liver ADHs (**Scheme 1**).<sup>15,25,49,50</sup> In this scheme, E and F represent the open and closed conformations of the enzyme.

**Scheme 1**



The open conformation of the apoenzyme with the inverted coordination of the catalytic zinc (E) binds NAD<sup>+</sup> to form the binary complex, E–NAD<sup>+</sup>, which then isomerizes to the closed conformation (F) with bound NAD<sup>+</sup> (F–NAD<sup>+</sup>). In this step, the subunit conformation closes, Arg-340 moves to interact with the coenzyme pyrophosphate and Glu-67, and Glu-67 OE2 is displaced from the zinc with water to form the classical coordination. Alcohol binds to make the F–NAD<sup>+</sup>–Alc complex, probably by a mechanism in which Glu-67 rebinds to the zinc, displacing the water, and then alcohol displaces Glu-67. In an alternative pathway, alcohol at high concentrations could bind directly to the E–NAD<sup>+</sup> complex, and the conformational change could be coupled to the change in zinc coordination. In the ternary complex (F–NAD<sup>+</sup>–Alc), the alcohol deprotonates to form the alkoxide (F–NAD<sup>+</sup>–Alk) via the hydrogen-bonded system, including Thr-45 OG1, nicotinamide ribose O2D, and His-48 ND1, with a rotation of the imidazole group. The *pro-R* hydrogen of the alcohol is transferred to the *re* face of the nicotinamide ring to produce the ternary complex with aldehyde and NADH (F–NADH–Ald). The aldehyde bound to the zinc is replaced with water when Glu-67 transiently binds to the zinc to produce the F–NADH complex; the conformation opens to form the E–NADH complex with the inverted coordination of the zinc, and NADH dissociates. An alternative pathway could bypass the F–NADH complex if aldehyde was simply displaced by Glu-67.

Structures for most of these species can be suggested: E (PDB entries 7KCQ and 4W6Z, subunits B and D), E–NAD<sup>+</sup> (PDB entry SENV, subunit B), F–NAD<sup>+</sup> (similar to *E. coli* ADH, PDB entry 5GKV), F–NAD<sup>+</sup>–Alk (PDB entries 7KCB and 4W6Z, subunits A and C; PDB entry SENV, subunit A), F–NADH (PDB entry 7KC2), and E–NADH (PDB entry 7KJY). The open structures of the E–NAD<sup>+</sup> and E–NADH complexes are very similar, as are the closed structures of the F–NAD<sup>+</sup> and F–NADH complexes. No structures for a complex of yeast ADH with NADH and aldehyde or an analogue (E–NADH–Ald) are available; however, some structures for the liver enzymes complexed with NADH and sulfoxides or formamides have been determined, and they are essentially identical to the complexes with NAD<sup>+</sup> and fluoroalcohols except for the nicotinamide ring and the ligands to the zinc.<sup>4,30,51–56</sup>

A simplified mechanism that illustrates the four relevant conformational and coordination states for the structures determined by cryo-EM is presented in the Graphical Abstract. The top two figures represent the open conformations with the inverted coordination of the zinc, and the bottom two are for the closed conformations and the classical coordination of the

zinc. The reverse catalytic reaction is shown. The apoenzyme (E) binds NADH to form the E–NADH complex, which isomerizes to form the F–NADH complex, which binds aldehyde (not shown, to form the E–NADH–Ald complex) and reduces it to form the F–NAD<sup>+</sup>–Alc complex, from which the products NAD<sup>+</sup> and alcohol dissociate (steps not shown) to form E. The oxidation of alcohol would proceed in the other direction with homologous conformational states for the enzyme–NAD<sup>+</sup> complexes (E–NAD<sup>+</sup> and F–NAD<sup>+</sup>).

The general mechanism in **Scheme 1** is also proposed to incorporate results on the structures and kinetics of dimeric horse liver ADH1E. X-ray structures of the ternary complexes of the tetrameric and dimeric ADHs all have the classical coordination of the catalytic zinc, but the apoenzyme forms of the dimeric enzymes have the classical coordination of the zinc, which requires additional steps to form the ternary complexes. Transient kinetic studies indicate that ADH1E binds NAD<sup>+</sup> and then deprotonates and changes conformation before other ligands bind to the zinc.<sup>57</sup> Binding of alcohol to the F–NAD<sup>+</sup> complex to make the F–NAD<sup>+</sup>–Alc complex probably involves the change in coordination of the zinc where Glu-67 binds to the zinc and displaces the water (or hydroxide), and the alcohol displaces Glu-67, as discussed previously.<sup>2,30</sup> As suggested above, the yeast enzyme could bypass this step if the alcohol binds directly to the inverted configuration of the zinc in the E–NAD<sup>+</sup> complex. Nevertheless, closed conformations with coenzyme and the classical coordination of the zinc with a water are observed for the homologous tetrameric yeast and *E. coli* enzymes (PDB entries 7KC2 and 4GKV<sup>43</sup>). At low concentrations of substrates, the ligand exchange mechanism with transient binding of the glutamate to the zinc might be the most feasible pathway.

Structures for several transient or intermediate states have not been determined. After alcohol binds to form the F–NAD<sup>+</sup>–Alc complex, deprotonation of the alcohol to form the F–NAD<sup>+</sup>–Alk ternary complex probably involves some local changes in the proton relay system. Molecular dynamics simulations for horse liver ADH provide some possible mechanisms for proton transfer.<sup>58–60</sup> The dissociation of aldehyde (F–NADH–Ald ⇌ F–NADH) also involves changes in zinc coordination. The structures of complexes with NADH in the closed (F–NADH) and open (E–NADH) conformations show two different states of zinc coordination, but the maps are not sufficient to determine intermediate states for zinc positions. Nevertheless, movement of the zinc to interact with Glu-68 (homologous to Glu-67 in yeast ADH) is evident in the structure of horse ADH complexed with NADH (PDB entry 4XD2).<sup>30</sup> In the cryo-EM structure of horse liver ADH complexed with NADH, it appears that the catalytic zinc has an inverted coordination and interacts with Glu-68 OE1 with distances of ~3.3 Å in the two subunits; however, this distance is longer than the value of 2.2 Å expected for direct ligation, and examination of the map and the 10 structural models suggests that the positioning is not certain.<sup>12</sup>

**Other Studies Relevant to the Proposed Mechanisms.** Quantum chemical and molecular mechanical calculations for models of horse liver ADH suggest that Glu-68 can intermittently coordinate to the zinc and facilitate exchange of water and substrates with favorable energetics.<sup>61</sup> The different coordinations of the zincs represent energetically accessible states, as implied by the observation that the two different conformations of yeast ADH bound to NADH can form under essentially the same conditions.

Substitution of Glu-67 in yeast ADH with glutamine decreases the catalytic efficiency ( $V/K_m$ , which includes the steps for substrate binding, hydride transfer, and product release) by 100-fold with both ethanol and acetaldehyde.<sup>16</sup> Affinities for coenzymes decrease modestly, but the affinity for trifluoroethanol decreases ~10-fold. Because isotope effects for ethanol oxidation ( $^D V$  and  $^D V/K_m \sim 2.6$ ) are less than intrinsic and pH-independent, we concluded that the substitution affects an isomerization in the ternary complex, which can be explained by the changes in conformation and coordination of the catalytic zinc observed for the yeast enzyme. A glutamine at residue 67 can fit into the active site in the open conformation, but the carboxyamido group would not coordinate well with the catalytic zinc in the closed state. Thus, the zinc in the E67Q enzyme could have the classical coordination observed in the horse liver apoenzyme with a water bound to the zinc; however, exchange of the water with the alcohol oxygen could be hindered if the zinc did not change coordination as readily, and the affinity for alcohols would be affected.

Transient kinetic studies provide some information about the proton transfer with the yeast enzyme. Mixing the enzyme with NAD<sup>+</sup> and trifluoroethanol in a stopped-flow spectrophotometer releases 0.5 H<sup>+</sup> per active site at pH 7.6 with a rate constant of 140 s<sup>-1</sup>, suggesting that the complex with NAD<sup>+</sup> and trifluoroethanol is probably deprotonated (i.e., as in F–NAD<sup>+</sup>–Alk above).<sup>50</sup> However, oxidation of 1-butanol has a turnover number of 20 s<sup>-1</sup> that is limited by hydride transfer in the ternary complex, and there was no significant proton release in the transient phase, suggesting that proton release occurs “at the same rate as NADH production”.<sup>50,62</sup> Oxidation of ethanol by yeast ADH has a turnover number of ~400 s<sup>-1</sup> at pH 7 and 25 °C, increasing above a pK of ~7.<sup>63,64</sup> Proton release in horse liver ADH differs from that in yeast ADH in that isomerization of the enzyme–NAD<sup>+</sup> complex is coupled to release of one proton per active site, and the conformational change (E–NAD<sup>+</sup> ⇌ F–NAD<sup>+</sup>) occurs before alcohols or other ligands bind.<sup>57,65</sup> The horse liver apoenzyme has the classical coordination of the zinc with Cys-46, His-67, Cys-174, and water (PDB entry 1YE3), and the water may deprotonate after NAD<sup>+</sup> binds. Although the zinc coordination in the yeast and horse apoenzymes differs, the mechanisms might proceed through similar steps with different rate constants for proton and hydride transfer.

Studies with human ADH3 (glutathione-dependent formaldehyde dehydrogenase) provide complementary information for a dimeric enzyme. The apoenzyme has the classical zinc coordination; however, complexes with adenosine diphosphoribose or NADH show crystallographic evidence for inversion of the coordination, and the abortive ternary complex with NADH and (S)-hydroxymethylglutathione has the classical zinc coordination.<sup>7,9,41,66</sup> Substituting Glu-67 with leucine in human ADH3 decreases the catalytic efficiency ( $V/K_m$ ) for oxidation of (S)-hydroxymethylglutathione by 3000-fold at pH 7.5, attributed to slower association of the substrate or an isomerization of a ternary complex. X-ray crystallography shows that the complex of E67L ADH3 with NADH has the classical coordination of the zinc, whereas the wild-type enzyme complex with NADH has the inverted coordination.<sup>66</sup>

The proposed role for Arg-340 in yeast ADH is supported by studies of two human ADHs with the homologous arginine. The R368L substitution in ADH3 decreases the catalytic efficiency with (S)-hydroxymethylglutathione by 3-fold but increases the turnover number by 8-fold due to weaker binding

and faster release of coenzyme. Relatively small (<1.6) deuterium kinetic isotope effects on  $V_1$  and  $V_1/K_m$  for oxidation of (S)-hydroxymethylglutathione by ADH3 and the mutated enzymes suggest that the enzyme–NAD<sup>+</sup>–(S)-hydroxymethylglutathione ternary complex isomerizes, which could be related to the inversion of the zinc coordination.

The naturally occurring isoenzyme of human ADH1B3 ( $\beta_3\beta_3$ ) has Arg-369 substituted with cysteine, and the affinity for NAD<sup>+</sup> is decreased by 350-fold, the rate of turnover ( $V_1$ ) for ethanol oxidation increased by 100-fold, and the catalytic efficiency decreased by 7-fold.<sup>67,68</sup> The three-dimensional structures of ternary complexes of ADH1B1 and ADH1B3 with NAD<sup>+</sup> and 4-iodopyrazole are the same, except that the side chain of Arg-369 is replaced with the cysteine and two waters in ADH1B3. Stopped-flow studies indicate that an isomerization of the enzyme–NADH complex might be rate-limiting for acetaldehyde reduction, as well as for ethanol oxidation.<sup>69</sup> Assigning a specific role for a particular amino acid in the enzymatic mechanism is problematic because several residues participate, but the structural evidence suggests that the binding of coenzyme is coupled to changes in the interaction of the glutamate with the arginine and the catalytic zinc.

## CONCLUSIONS

The cryo-EM studies confirm that yeast ADH1 has two major conformational states where the coordination of the catalytic zinc changes in response to the binding of coenzyme. Cryo-EM shows that the apoenzyme and one binary complex with NADH have the open conformation and the inverted coordination of the zinc with Glu-67, whereas another binary complex with NADH and the ternary complex with NAD<sup>+</sup> and trifluoroethanol have the closed conformation and the classical coordination of the zinc with water or alcohol. All structures are symmetric tetramers, whereas X-ray crystallography revealed asymmetry in the dimeric units, which could arise because of crystal lattice contacts. The cryo-EM structures suggest that each subunit can act independently, but further studies might show evidence for cooperativity in catalysis because of quaternary interactions. The complementary methods provide structures for energetically accessible states that are relevant for catalysis.

Coordination of the catalytic zinc and subunit conformations in alcohol dehydrogenases change during the catalytic reaction. A general observation is that apoenzyme forms of dimeric ADHs have the classical coordination of the catalytic zinc and evidence of inversion at the zinc when coenzymes bind. The apoenzymes of the tetrameric enzymes have the inverted coordination of the catalytic zinc, and binding of coenzyme can result in inversion of the coordination. The ternary complexes with coenzymes and substrate analogues for zinc-dependent dehydrogenases have the classical coordination. How the quaternary structures affect the zinc coordination is not clear. Nevertheless, it appears that similar structural changes may facilitate catalysis by common mechanisms.

## ASSOCIATED CONTENT

### Accession Codes

Structural data have been deposited in the RCSB as entries 7KCQ, 7KJY, 7KC2, and 7KCB.

## AUTHOR INFORMATION

### Corresponding Author

Ramaswamy Subramanian – Department of Biological Sciences and Weldon School of Biomedical Engineering, Purdue University, West Lafayette, Indiana 47907, United States;  orcid.org/0000-0002-6709-190X;  
Email: subram68@purdue.edu

### Authors

Sai Rohit Guntupalli – Institute for Stem Cell Science and Regenerative Medicine, Bangalore, India; Manipal University, Manipal, India; Department of Biological Sciences, Purdue University, West Lafayette, Indiana 47907, United States  
Zhuang Li – Department of Biological Sciences, Purdue University, West Lafayette, Indiana 47907, United States  
Leifu Chang – Department of Biological Sciences, Purdue University, West Lafayette, Indiana 47907, United States  
Bryce V. Plapp – Department of Biochemistry, Bowen Science Building, The University of Iowa, Iowa City, Iowa 52242, United States;  orcid.org/0000-0001-6790-5363

Complete contact information is available at:  
<https://pubs.acs.org/10.1021/acs.biochem.0c00921>

### Author Contributions

#S.R.G. and L.Z. contributed equally to this work.

### Funding

This work was supported by grants from Purdue University, West Lafayette, IN (to S.R.G.), and by National Institutes of Health Grants R01GM138675 (to L.C.) and R01GM078446 (to B.V.P.).

### Notes

The authors declare no competing financial interest.

## ABBREVIATIONS

ADH, alcohol dehydrogenase; ScbADH, *S. carlsbergensis* ADH; TFE, 2,2,2-trifluoroethanol; cryo-EM, cryogenic electron microscopy.

## REFERENCES

- (1) Savarimuthu, B. R., Ramaswamy, S., and Plapp, B. V. (2014) Yeast alcohol dehydrogenase structure and catalysis. *Biochemistry* 53, 5791–5803.
- (2) Plapp, B. V., Charlier, H. A., Jr., and Ramaswamy, S. (2016) Mechanistic implications from structures of yeast alcohol dehydrogenase complexed with coenzyme and an alcohol. *Arch. Biochem. Biophys.* 591, 35–42.
- (3) Eklund, H., Nordström, B., Zeppezauer, E., Söderlund, G., Ohlsson, I., Boiwe, T., Söderberg, B. O., Tapia, O., Brändén, C.-I., and Åkeson, Å (1976) Three-dimensional structure of horse liver alcohol dehydrogenase at 2.4 Å resolution. *J. Mol. Biol.* 102, 27–59.
- (4) Eklund, H., Samama, J. P., Wallén, L., Brändén, C. I., Åkeson, Å., and Jones, T. A. (1981) Structure of a triclinic ternary complex of horse liver alcohol dehydrogenase at 2.9 Å resolution. *J. Mol. Biol.* 146, 561–587.
- (5) Eklund, H., and Ramaswamy, S. (2008) Medium- and short-chain dehydrogenase/reductase gene and protein families: Three-dimensional structures of MDR alcohol dehydrogenases. *Cell. Mol. Life Sci.* 65, 3907–3917.
- (6) Sun, H. W., and Plapp, B. V. (1992) Progressive sequence alignment and molecular evolution of the Zn-containing alcohol-dehydrogenase family. *J. Mol. Evol.* 34, 522–535.
- (7) Yang, Z. N., Bosron, W. F., and Hurley, T. D. (1997) Structure of human  $\alpha\beta$  alcohol dehydrogenase: a glutathione-dependent formaldehyde dehydrogenase. *J. Mol. Biol.* 265, 330–343.
- (8) Karlsson, A., El-Ahmad, M., Johansson, K., Shafqat, J., Jörnvall, H., Eklund, H., and Ramaswamy, S. (2003) Tetrameric NAD-dependent alcohol dehydrogenase. *Chem.-Biol. Interact.* 143–144, 239–245.
- (9) Sanghani, P. C., Robinson, H., Bosron, W. F., and Hurley, T. D. (2002) Human glutathione-dependent formaldehyde dehydrogenase. Structures of apo, binary, and inhibitory ternary complexes. *Biochemistry* 41, 10778–10786.
- (10) Brändén, C. I., Jörnvall, H., Eklund, H., and Furugen, B. (1975) Alcohol Dehydrogenases. *The Enzymes*, 3rd Ed. 11, 103–190.
- (11) Valencia, E., Larroy, C., Ochoa, W. F., Parés, X., Fita, I., and Biosca, J. A. (2004) Apo and Holo structures of an NADPH-dependent cinnamyl alcohol dehydrogenase from *Saccharomyces cerevisiae*. *J. Mol. Biol.* 341, 1049–1062.
- (12) Herzik, M. A., Jr., Wu, M., and Lander, G. C. (2019) High-resolution structure determination of sub-100 kDa complexes using conventional cryo-EM. *Nat. Commun.* 10, 1032.
- (13) Pal, S., Park, D. H., and Plapp, B. V. (2009) Activity of yeast alcohol dehydrogenases on benzyl alcohols and benzaldehydes. Characterization of ADH1 from *Saccharomyces carlsbergensis* and transition state analysis. *Chem.-Biol. Interact.* 178, 16–23.
- (14) Walker, J. M. (1994) Gradient SDS polyacrylamide gel electrophoresis of proteins. *Methods Mol. Biol.* 32, 35–38.
- (15) Ganzhorn, A. J., Green, D. W., Hershey, A. D., Gould, R. M., and Plapp, B. V. (1987) Kinetic characterization of yeast alcohol dehydrogenases. Amino acid residue 294 and substrate specificity. *J. Biol. Chem.* 262, 3754–3761.
- (16) Ganzhorn, A. J., and Plapp, B. V. (1988) Carboxyl groups near the active site zinc contribute to catalysis in yeast alcohol dehydrogenase. *J. Biol. Chem.* 263, 5446–5454.
- (17) Suloway, C., Pulokas, J., Fellmann, D., Cheng, A., Guerra, F., Quispe, J., Stagg, S., Potter, C. S., and Carragher, B. (2005) Automated molecular microscopy: the new Leginon system. *J. Struct. Biol.* 151, 41–60.
- (18) Zivanov, J., Nakane, T., Forsberg, B. O., Kimanius, D., Hagen, W. J., Lindahl, E., and Scheres, S. H. (2018) New tools for automated high-resolution cryo-EM structure determination in RELION-3. *eLife*, e42166.
- (19) Zheng, S. Q., Palovcak, E., Armache, J. P., Verba, K. A., Cheng, Y., and Agard, D. A. (2017) MotionCor2: anisotropic correction of beam-induced motion for improved cryo-electron microscopy. *Nat. Methods* 14, 331–332.
- (20) Zhang, K. (2016) Gctf: Real-time CTF determination and correction. *J. Struct. Biol.* 193, 1–12.
- (21) Punjani, A., Rubinstein, J. L., Fleet, D. J., and Brubaker, M. A. (2017) cryoSPARC: algorithms for rapid unsupervised cryo-EM structure determination. *Nat. Methods* 14, 290–296.
- (22) Liebschner, D., Afonine, P. V., Baker, M. L., Bunkoczi, G., Chen, V. B., Croll, T. I., Hintze, B., Hung, L. W., Jain, S., McCoy, A. J., Moriarty, N. W., Oeffner, R. D., Poon, B. K., Prisant, M. G., Read, R. J., Richardson, J. S., Richardson, D. C., Sammito, M. D., Sobolev, O. V., Stockwell, D. H., Terwilliger, T. C., Urzhumtsev, A. G., Videau, L. L., Williams, C. J., and Adams, P. D. (2019) Macromolecular structure determination using X-rays, neutrons and electrons: recent developments in Phenix. *Acta Crystallogr. D: Struct. Biol.* 75, 861–877.
- (23) Emsley, P., Lohkamp, B., Scott, W. G., and Cowtan, K. (2010) Features and development of Coot. *Acta Crystallogr., Sect. D: Biol. Crystallogr.* 66, 486–501.
- (24) Rossmann, M. G., Liljas, A., Brändén, C.-I., and Banaszak, L. J. (1975) Evolutionary and structural relationships among dehydrogenases. *The Enzymes*, 3rd Ed. 11, 61–102.
- (25) Dickenson, C. J., and Dickinson, F. M. (1978) Inhibition by ethanol, acetaldehyde and trifluoroethanol of reactions catalysed by yeast and horse liver alcohol dehydrogenases. *Biochem. J.* 171, 613–627.
- (26) Shearer, G. L., Kim, K., Lee, K. M., Wang, C. K., and Plapp, B. V. (1993) Alternative pathways and reactions of benzyl alcohol and benzaldehyde with horse liver alcohol dehydrogenase. *Biochemistry* 32, 11186–11194.

- (27) Charlier, H. A., Jr., and Plapp, B. V. (2000) Kinetic cooperativity of human liver alcohol dehydrogenase gamma(2). *J. Biol. Chem.* 275, 11569–11575.
- (28) Levin, I., Meiri, G., Peretz, M., Burstein, Y., and Frolow, F. (2004) The ternary complex of *Pseudomonas aeruginosa* alcohol dehydrogenase with NADH and ethylene glycol. *Protein Sci.* 13, 1547–1556.
- (29) Rubach, J. K., and Plapp, B. V. (2003) Amino acid residues in the nicotinamide binding site contribute to catalysis by horse liver alcohol dehydrogenase. *Biochemistry* 42, 2907–2915.
- (30) Plapp, B. V., Savarimuthu, B. R., Ferraro, D. J., Rubach, J. K., Brown, E. N., and Ramaswamy, S. (2017) Horse liver alcohol dehydrogenase: zinc coordination and catalysis. *Biochemistry* 56, 3632–3646.
- (31) Jones, T. A., Zou, J. Y., Cowan, S. W., and Kjeldgaard, M. (1991) Improved methods for building protein models in electron density maps and the location of errors in these models. *Acta Crystallogr., Sect. A: Found. Crystallogr.* A47, 110–119.
- (32) Yahashiri, A., Rubach, J. K., and Plapp, B. V. (2014) Effects of cavities at the nicotinamide binding site of liver alcohol dehydrogenase on structure, dynamics and catalysis. *Biochemistry* 53, 881–894.
- (33) Shanmuganathan, K. K., Wallace, R. S., Lee, A. T.-I., and Plapp, B. V. (2018) Contribution of buried distal amino acid residues in horse liver alcohol dehydrogenase to structure and catalysis. *Protein Sci.* 27, 750–768.
- (34) Brandes, N., Reichmann, D., Tienson, H., Leichert, L. I., and Jakob, U. (2011) Using quantitative redox proteomics to dissect the yeast redoxome. *J. Biol. Chem.* 286, 41893–41903.
- (35) De Bolle, X., Vinals, C., Prozzi, D., Paquet, J. Y., Leplae, R., Depiereux, E., Vandenhautte, J., and Feytmans, E. (1995) Identification of residues potentially involved in the interactions between subunits in yeast alcohol dehydrogenases. *Eur. J. Biochem.* 231, 214–219.
- (36) Künkel, W., Hädrich, H., Damaschun, H., and Damaschun, G. (1980) Alkoholdehydrogenase (ADH) in Hefezellen. III. Strukturerorschungen an zellulären ADH-Kristallen von *Saccharomyces carlsbergensis* mit Hilfe der Elektronenmikroskopie und Röntgenkleinkinkelstreuung. *Mikroskopie* 36, 81–92.
- (37) Lange, R. H. (1981) Alkoholdehydrogenase (ADH) aus Hefe. Eine Krystallographische Interpretation. *Mikroskopie* 38, 78–80.
- (38) Colonna-Cesari, F., Perahia, D., Karplus, M., Eklund, H., Brändén, C.-I., and Tapia, O. (1986) Interdomain motion in liver alcohol dehydrogenase. Structural and energetic analysis of the hinge bending mode. *J. Biol. Chem.* 261, 15273–15280.
- (39) Plapp, B. V., and Ramaswamy, S. (2012) Atomic-resolution structures of horse liver alcohol dehydrogenase with NAD<sup>+</sup> and fluoroalcohols define strained Michaelis complexes. *Biochemistry* 51, 4035–4048.
- (40) Ramaswamy, S., El-Ahmad, M., Danielsson, O., Jörnvall, H., and Eklund, H. (1996) Crystal structure of cod liver class I alcohol dehydrogenase: substrate pocket and structurally variable segments. *Protein Sci.* 5, 663–671.
- (41) Sanghani, P. C., Bosron, W. F., and Hurley, T. D. (2002) Human glutathione-dependent formaldehyde dehydrogenase. Structural changes associated with ternary complex formation. *Biochemistry* 41, 15189–15194.
- (42) Chen, F., Wang, P., An, Y., Huang, J., and Xu, Y. (2015) Structural insight into the conformational change of alcohol dehydrogenase from *Arabidopsis thaliana* L. during coenzyme binding. *Biochimie* 108, 33–39.
- (43) Thomas, L. M., Harper, A. R., Miner, W. A., Ajufo, H. O., Brascum, K. M., Kao, L., and Sims, P. A. (2013) Structure of *Escherichia coli* AdhP (ethanol-inducible dehydrogenase) with bound NAD. *Acta Crystallogr., Sect. F: Struct. Biol. Cryst. Commun.* F69, 730–732.
- (44) Ceccarelli, C., Liang, Z. X., Strickler, M., Prehna, G., Goldstein, B. M., Klinman, J. P., and Bahnsen, B. J. (2004) Crystal structure and amide H/D exchange of binary complexes of alcohol dehydrogenase from *Bacillus stearothermophilus*: insight into thermostability and cofactor binding. *Biochemistry* 43, 5266–5277.
- (45) Esposito, L., Sica, F., Raia, C. A., Giordano, A., Rossi, M., Mazzarella, L., and Zagari, A. (2002) Crystal structure of the alcohol dehydrogenase from the hyperthermophilic archaeon *Sulfolobus solfataricus* at 1.85 Å resolution. *J. Mol. Biol.* 318, 463–477.
- (46) Esposito, L., Bruno, I., Sica, F., Raia, C. A., Giordano, A., Rossi, M., Mazzarella, L., and Zagari, A. (2003) Crystal structure of a ternary complex of the alcohol dehydrogenase from *Sulfolobus solfataricus*. *Biochemistry* 42, 14397–14407.
- (47) Guy, J. E., Isupov, M. N., and Littlechild, J. A. (2003) The structure of an alcohol dehydrogenase from the hyperthermophilic archaeon *Aeropyrum pernix*. *J. Mol. Biol.* 331, 1041–1051.
- (48) Kang, C., Hayes, R., Sanchez, E. J., Webb, B. N., Li, Q., Hooper, T., Nissen, M. S., and Xun, L. (2012) Furfural reduction mechanism of a zinc-dependent alcohol dehydrogenase from *Cupriavidus necator* JMP134. *Mol. Microbiol.* 83, 85–95.
- (49) Wratten, C. C., and Cleland, W. W. (1963) Product inhibition studies on yeast and liver alcohol dehydrogenases. *Biochemistry* 2, 935–941.
- (50) Dickinson, F. M., and Dickenson, C. J. (1978) Estimation of rate and dissociation constants involving ternary complexes in reactions catalysed by yeast alcohol dehydrogenase. *Biochem. J.* 171, 629–637.
- (51) Al-Karadaghi, S., Cedergren-Zeppezauer, E. S., Hovmøller, S., Petratos, K., Terry, H., and Wilson, K. S. (1994) Refined crystal structure of liver alcohol dehydrogenase NADH complex at 1.8-Å Angstrom resolution. *Acta Crystallogr., Sect. D: Biol. Crystallogr.* 50, 793–807.
- (52) Meijers, R., Adolph, H. W., Dauter, Z., Wilson, K. S., Lamzin, V. S., and Cedergren-Zeppezauer, E. S. (2007) Structural evidence for a ligand coordination switch in liver alcohol dehydrogenase. *Biochemistry* 46, 5446–5454.
- (53) Cho, H., Ramaswamy, S., and Plapp, B. V. (1997) Flexibility of liver alcohol dehydrogenase in stereoselective binding of 3-butylthiolane 1-oxides. *Biochemistry* 36, 382–389.
- (54) Ramaswamy, S., Scholze, M., and Plapp, B. V. (1997) Binding of formamides to liver alcohol dehydrogenase. *Biochemistry* 36, 3522–3527.
- (55) Venkataramaiah, T. H., and Plapp, B. V. (2003) Formamides mimic aldehydes and inhibit liver alcohol dehydrogenases and ethanol metabolism. *J. Biol. Chem.* 278, 36699–36706.
- (56) Gibbons, B. J., and Hurley, T. D. (2004) Structure of three class I human alcohol dehydrogenases complexed with isoenzyme specific formamide inhibitors. *Biochemistry* 43, 12555–12562.
- (57) Kovaleva, E. G., and Plapp, B. V. (2005) Deprotonation of the horse liver alcohol dehydrogenase-NAD<sup>+</sup> complex controls formation of the ternary complexes. *Biochemistry* 44, 12797–12808.
- (58) Agarwal, P. K., Webb, S. P., and Hammes-Schiffer, S. (2000) Computational studies of the mechanism for proton and hydride transfer in liver alcohol dehydrogenase. *J. Am. Chem. Soc.* 122, 4803–4812.
- (59) Luo, J., and Bruice, T. C. (2001) Dynamic structures of horse liver alcohol dehydrogenase (HLADH): Results of molecular dynamics simulations of HLADH-NAD<sup>+</sup>-PhCH<sub>2</sub>OH, HLADH-NAD<sup>+</sup>-PhCH<sub>2</sub>O<sup>−</sup>, and HLADH-NADH-PhCHO. *J. Am. Chem. Soc.* 123, 11952–11959.
- (60) Cui, Q., Elstner, M., and Karplus, M. (2002) A theoretical analysis of the proton and hydride transfer in liver alcohol dehydrogenase (LADH). *J. Phys. Chem. B* 106, 2721–2740.
- (61) Ryde, U. (1995) On the role of Glu-68 in alcohol dehydrogenase. *Protein Sci.* 4, 1124–1132.
- (62) Dickenson, C. J., and Dickinson, F. M. (1975) A study of the oxidation of butan-1-ol and propan-2-ol by nicotinamide-adenine dinucleotide catalysed by yeast alcohol dehydrogenase. *Biochem. J.* 147, 541–547.
- (63) Dickenson, C. J., and Dickinson, F. M. (1975) A study of the pH- and temperature-dependence of the reactions of yeast alcohol

dehydrogenase with ethanol, acetaldehyde and butyraldehyde as substrates. *Biochem. J.* 147, 303–311.

(64) Gould, R. M., and Plapp, B. V. (1990) Substitution of arginine for histidine-47 in the coenzyme binding site of yeast alcohol dehydrogenase I. *Biochemistry* 29, 5463–5468.

(65) Sekhar, V. C., and Plapp, B. V. (1990) Rate constants for a mechanism including intermediates in the interconversion of ternary complexes by horse liver alcohol dehydrogenase. *Biochemistry* 29, 4289–4295.

(66) Sanghani, P. C., Davis, W. I., Zhai, L., and Robinson, H. (2006) Structure-function relationships in human glutathione-dependent formaldehyde dehydrogenase. Role of Glu-67 and Arg-368 in the catalytic mechanism. *Biochemistry* 45, 4819–4830.

(67) Burnell, J. C., Li, T. K., and Bosron, W. F. (1989) Purification and steady-state kinetic characterization of human liver beta 3 beta 3 alcohol dehydrogenase. *Biochemistry* 28, 6810–6815.

(68) Davis, G. J., Bosron, W. F., Stone, C. L., Owusu-Dekyi, K., and Hurley, T. D. (1996) X-ray structure of human beta(3)beta(3) alcohol dehydrogenase - The contribution of ionic interactions to coenzyme binding. *J. Biol. Chem.* 271, 17057–17061.

(69) Stone, C. L., Jipping, M. B., Owusu-Dekyi, K., Hurley, T. D., Li, T. K., and Bosron, W. F. (1999) The pH-dependent binding of NADH and subsequent enzyme isomerization of human liver beta 3 beta 3 alcohol dehydrogenase. *Biochemistry* 38, 5829–5835.